Available online at www.sciencedirect.com
ScienceDirect
Journal of Magnetic Resonance 188 (2007) 206–215
JMR Journal of Magnetic Resonance
www.elsevier.com/locate/jmr

Nuclear spin resonance of ^{129}Xe doped with O_2

J.W. McNabb [1], D.N. Balakishiyeva, A. Honig *

Physics Department, Syracuse University, Syracuse, NY 13244, USA

Received 28 March 2007; revised 28 June 2007
Available online 17 July 2007

Abstract

Spin–lattice relaxation of ^{129}Xe nuclei in solid natural xenon has been investigated in detail over a large range of paramagnetic O_2 impurity concentrations. Direct measurements of the ground state magnetic properties of the O_2 are difficult because the ESR (electron spin resonance) lines of O_2 are rather unstructured, but NMR measurements in the liquid helium temperature region (1.4–4 K) are very sensitive to the effective magnetic moments associated with the spin 1 Zeeman levels of the O_2 molecules and to the O_2 magnetic relaxation. From these measurements, the value of the $D[Sz^2 - (1/3)S^2]$ spin-Hamiltonian term of the triplet spin ground state of O_2 can be determined. The temperature and magnetic field dependence of the measured paramagnetic O_2-induced excess line width of the ^{129}Xe NMR signal agree well with the theoretical model with the spin-Hamiltonian $D = 0.19$ meV (2.3 K), and with the reasonable assumption that the $E[S_x^2 - S_y^2]$ spin-Hamiltonian term is close to 0 meV. An anomalous temperature dependence between 1.4 K and 4.2 K of the ^{129}Xe spin–lattice relaxation rate, $T_{1n}^{-1}(T)$, is also accounted for by our model. Using an independent determination of the true O_2 concentration in the Xe–O_2 solid, the effective spin lattice relaxation time (which will be seen to be transition dependent) of the O_2 at 2.3 K and 0.96 T is determined to be approximately 1.4×10^{-8} s. The experimental results, taken together with the relaxation model, suggest routes for bringing highly spin-polarized ^{129}Xe from the low temperature condensed phase to higher temperatures without excessive depolarization.

Keywords: Nuclear spin relaxation; O_2 impurities; Solid xenon; Hyperpolarized ^{129}Xe; MRI

1. Introduction

The systematic investigation of spin–lattice relaxation of ^{129}Xe in solid mixtures of xenon and oxygen is of special interest since it governs one part of a cycle which has been proposed [1] to produce hyperpolarized ^{129}Xe in the condensed state. Hyperpolarized ^{129}Xe, defined as having a nuclear magnetization in excess of its thermal equilibrium value at a given temperature and magnetic field, is currently produced in the gaseous state by an optical pumping and spin exchange method [2]. With polarization near unity attainable, the enhancement factor at room temperature and ~1 T magnitude fields is roughly 10^5. With the system at temperature T and magnetic field B the non-equilibrium hyperpolarization decays at the nuclear spin–lattice relaxation rate, $T_{1n}^{-1}(T, B)$. Owing to ^{129}Xe's spin 1/2 and small magnetic moment, the relaxation is slow and the hyperpolarization at room temperature and atmospheric pressure persists for several hours for pure gas and for many minutes for typically O_2 contaminated gas, enabling use as a contrast agent [3] for magnetic resonance imaging (MRI). At lower temperatures where the polarization can persist for hours to days, other applications related to quantum computation [4] and employment of large xenon targets [5] are feasible. It is not difficult to conceive of interesting applications of large hyperpolarized xenon targets, for nuclear physics and for possible dark matter detection. The MRI application, which of course has been realized for over a decade, requires substantial material for an image set for lungs, of the order of a liter at room temperature and atmospheric pressure, and large polarized xenon targets require even more. Production in the condensed

* Corresponding author. Fax: +1 315 443 9103.
E-mail address: honig@phy.syr.edu (A. Honig).
[1] Present address: Intel Corporation, Hillsboro, OR, USA.

1090-7807/$ - see front matter © 2007 Elsevier Inc. All rights reserved.
doi:10.1016/j.jmr.2007.07.002

state holds promise of generating the hyperpolarized material [6] more copiously and economically than with the gaseous phase optical pumping procedures.

A direct way to achieve high polarization in the condensed state is via thermal equilibrium at mK temperatures and multi-tesla magnetic fields. For the polarization to build up towards equilibrium in a reasonable time, for example the order of a day, a relaxation catalyst is required. In preliminary experiments [1], molecular oxygen, which at dilute concentrations in a diamagnetic host is paramagnetic in its ground state, serves this function. At a nominal concentration of 4%, which recalibrates to 6×10^{-3} mole fraction O_2 using the results in this paper and T_1(1 T, 1.4 K) data common to both experiments, at 30 mK and 12 T a polarization of about 0.1 was obtained in one day. This value is significant, and improvements in the catalyst may allow polarizations nearer to the 0.5 equilibrium value at 10 mK and 20 T to be attained. For the hyperpolarization to survive for use at higher temperatures, the relaxation agent, in this case oxygen, must be switched off [1,6] so that depolarization does not occur prematurely. One way to achieve this is by removal of sufficient oxygen during the warm-up process. The polarizing portion of the cycle has already been demonstrated [1], but polarization retention during warm-up and oxygen catalyst removal at feasible warm-up rates depends on the ^{129}Xe spin relaxation rates, T_{1n}^{-1}, as a function of oxygen concentration, temperature and magnetic field. This T_1 behavior is elucidated in this investigation, and it is shown that there are parameter windows in the concentration, T, and B domains in which a relaxation switch can operate satisfactorily between 1.4 K and the temperature of a final polarized liquid or gas. A simple demonstration indicated that for modest oxygen mole fraction of about 10^{-3} [T_1(1 T, 1.4 K) ~200 s], hyperpolarized xenon with an enhancement of 10^2 was obtained upon raising T from 1.4 K to 150 K, even without oxygen extraction. Although this O_2 mole fraction is a factor of 6 lower than the corrected value in the experiment of Ref. [1] which yielded 10% polarization, its T_1 could be made comparable at $B = 10$ T, assuming the linear dependence of T_1 on B in this region. An attractive alternative to the dilution refrigerator mK phase for reaching high equilibrium polarization is dynamic nuclear polarization (DNP) of the ^{129}Xe at temperatures in the 0.4–1.4 K range, followed by the warm-up phase, a goal being actively pursued.

2. Methods and scope of investigation

Oxygen is a well-known paramagnetic impurity which has frequently served to increase nuclear spin relaxation rates [7] in many systems. There have been several detailed studies of nuclear spin relaxation in pure xenon, and the effect of oxygen in reducing its spin–lattice relaxation time has been observed [8,9]. However, systematic studies do not appear to have been undertaken over a wide range of temperature, magnetic field, and oxygen concentrations. Although our original goal was to determine applicability of O_2-induced relaxation to large effective hyperpolarization, our investigations revealed interesting and unanticipated effects at the low temperatures (liquid helium region) bearing on the magnetic energy state structure of O_2 molecules in solid xenon hosts. The ^{129}Xe NMR line width is narrow (0.03 mT) in the solid even at temperatures far below the near-melting point region of rapid self diffusion, and hence is sensitive to local field increments arising from fairly low concentrations of paramagnetic O_2. As a result, quantitative measurements of susceptibility in the 1.4–4 K region yielded a determination of the crystal field splitting parameter [10] D of the spin-Hamiltonian term $D[Sz^2 - (1/3)S^2]$, associated with the oxygen triplet state, under the reasonable assumption that the E term is near zero. This is frequently the case for symmetric molecules, and implied in our case by the excellent data fit using a single value of D. The line width measurements also serve to calibrate the oxygen concentration, from which the effectiveness of various protocols for matrix isolation mixing of oxygen in solid xenon become testable. In previous investigations [11], oxygen doped rare gases have been condensed into a matrix isolated solid. An initial gas mixture of the rare gas and the oxygen was quickly frozen, trapping the oxygen in the solid. We used this method for a few doping concentrations, but for most of our experiments, we condensed Xe–O_2 mixtures first to a liquid, followed by moderately rapid (3–10 min) freezing. This gave a better sample generally, with an intrinsic line width narrower than in the former case. A complication associated with condensation arises from the vapor barrier [12] of the non-condensable O_2 gas, but our results indicate this does not impede the ability to prepare matrix isolated Xe–O_2 solids with reproducible oxygen concentrations. Both the line width measurements and the spin–lattice relaxation rates of the ^{129}Xe nuclei, T_{1n}^{-1}, measured at liquid helium temperatures where the spin–lattice relaxation is due almost entirely to O_2, support the contention that solid Xe–O_2 mixtures repeatably are prepared with mole fractions closely proportional to those of the initial gas mixture. We also experimentally demonstrated with direct measurements that for our condensed sample preparation method which proceeds through the liquid phase, the true mole fraction of O_2 in the condensed Xe–O_2 solid is 0.32 of the initial mole fraction of the initial gas mixture. Further consideration of these aspects is given in Section 6.

3. ^{129}Xe spin–lattice relaxation rates

For the NMR measurements, we used a standard home-built crossed-coil NMR low temperature probe system, with field-swept continuous wave NMR measurements. An electromagnet provides a homogeneous field up to 1.1 T. The gas mixture sample is condensed into a glass cylinder of 9 mm diameter to form a volume of solid of about 2 cm^3. A typical signal to noise ratio for ^{129}Xe at thermal equilibrium at 4 K and 1 T is 100. In Fig. 1a, the ^{129}Xe

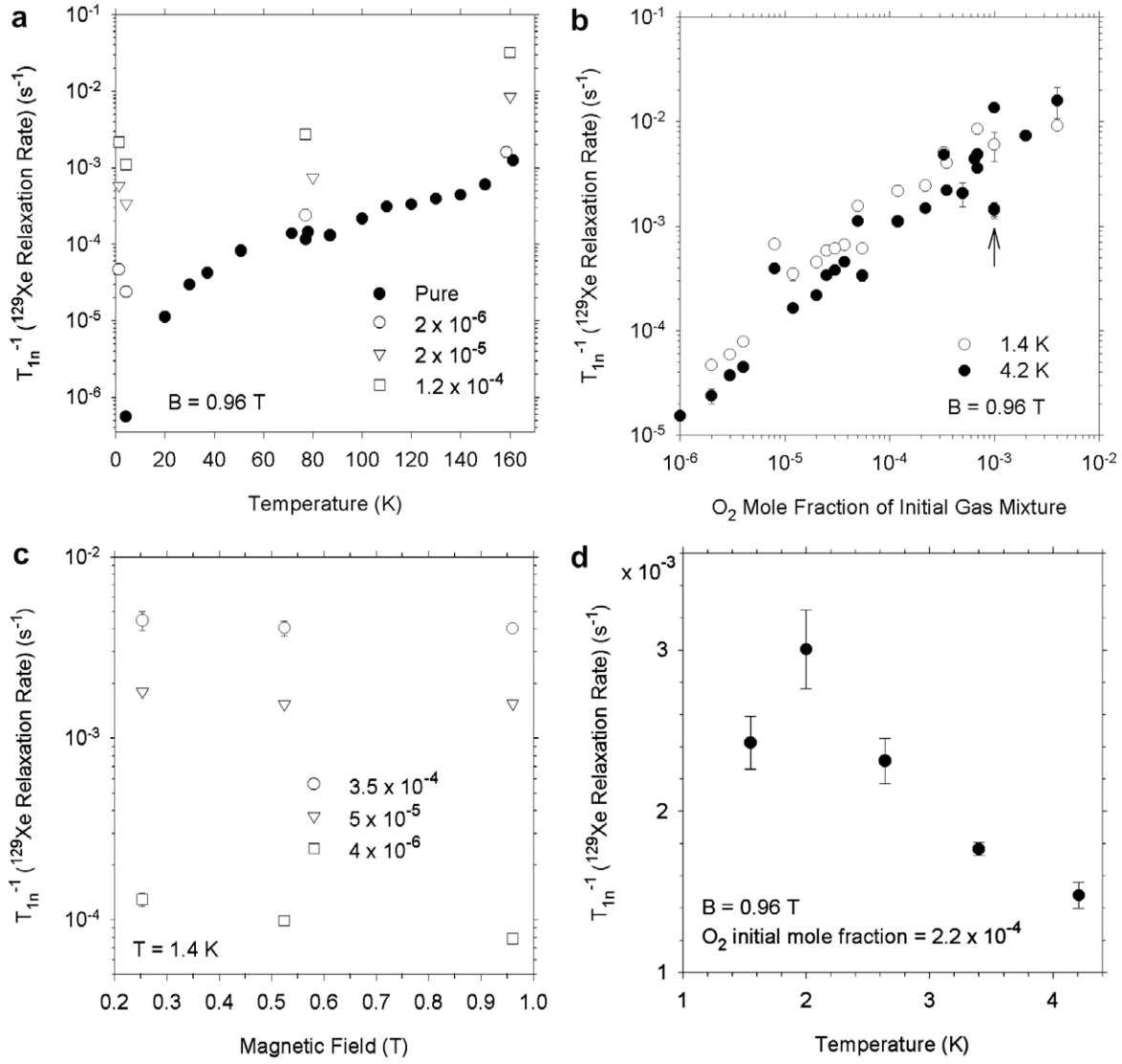

Fig. 1. (a) Overview of temperature dependence of T_1 (^{129}Xe) for O_2-doped xenon in the solid phase. Pure sample data is from Ref. [13]. For initial mixture O_2 mole fraction $>2\times10^{-6}$ the O_2 impurity relaxation dominates T_{1n}^{-1} (^{129}Xe) throughout the temperature range. The small increase of T_{1n}^{-1} (^{129}Xe) at 1 K over its value at 4 K is a real effect, consistent at all O_2 concentrations, and discussed in the text. (b) Illustration of approximately linear dependence of O_2-induced T_{1n}^{-1} (^{129}Xe) on initial mixture O_2 mole fraction at 1.4 K and 4.2 K. Arrow denotes sample condensed rapidly from the gas mixture. (c) Plot of T_{1n}^{-1} against B, for three different initial mixture O_2 mole fractions. (d) Temperature dependence of T_{1n}^{-1} for one sample in the low temperature region.

relaxation rate, T_{1n}^{-1}, is plotted as a function of temperature for several values of the initial mole fraction of O_2 in the xenon–oxygen gas mixture, which is the experimentally measured quantity in each experiment. As already pointed out, the true O_2 mole fraction in the sample is 0.32× the initial mixture value, determined from separate experiments described in Section 6. In the higher temperature region above about 120 K, the relaxation is dominated by an intrinsic vacancy mechanism [13], but in the low temperature region, for an initial mixture oxygen mole fraction exceeding 5×10^{-6}, the oxygen impurity relaxation mechanism dominates over the intrinsic relaxation. The oxygen-induced relaxation rate is also noted to be approximately proportional to the oxygen concentration. This linear dependence on oxygen concentration in the 1.4–4.2 K temperature range is indicative of the proportionality of the true concentration in the solid to the initial mole fraction of oxygen in the xenon–oxygen gas mixture. Such a nuclear spin-relaxation dependence on the concentration of paramagnetic impurities has been seen in other systems, for example methane [14] doped with O_2. It is an expected result when spin diffusion [15] is an essential factor in the relaxation of the magnetization of the nuclei. In Fig. 1b, the relaxation rate excess over the intrinsic ('zero' O_2 concentration) is plotted for 1.4 K and 4.2 K. A single point which corresponds to sample condensation directly from the gas mixture onto a cold (77 K) surface is indicated by an arrow, but the majority of points correspond to condensation into the liquid state followed by a moderately rapid freeze of duration about 3–10 min, where the linear relationship holds quite well. For direct condensation to the solid, a somewhat smaller fraction of the initial mixture

O_2 mole fraction gets incorporated into the solid. These issues will be further discussed in Section 6. From both Fig. 1a and b, it is noteworthy that consistently and well outside the experimental error, T_{1n}^{-1} at 1.4 K is faster than at 4.2 K. We will return to this anomalous feature after a model, based upon our measurements, is established for the magnetic state structure of the O_2 molecule in solid xenon.

The magnetic field dependence of the relaxation rate at 1.4 K is shown in Fig. 1c for three magnetic field values between 0.2 T and 1 T for 3 relatively low initial gas mixture O_2 mole fractions, where T_{1n} is long enough for field dependent relaxation measurements to be made at a single resonance frequency, using a field cycling technique in which the field is switched from "measurement" value to "relaxation" value in a time $t \ll T_{1n}$. For higher concentrations, where T_{1n} is shorter than 5 min, the NMR measurement frequency is re-tuned to resonate at the appropriate field, over a field range of 0.2–1 T. The conclusion we draw from both methods is that the relaxation is nearly independent of magnetic field. We defer the comparison of that result with theory until the relaxation model is presented and examined, but indicate here that it strongly defines what is called the "fast diffusion" mode of paramagnetic-impurity-induced nuclear spin relaxation.

The temperature dependence of the spin–lattice relaxation rate for a sample of initial mixture O_2 mole fraction of about 2.2×10^{-4} is shown in Fig. 1d. The anomalous inversion of relaxation rate dependence on temperature in the 1–4 K region, already noted in Fig. 1a, is seen in more detail here. A maximum occurs near 2 K, the origin of which will be explained and analyzed quantitatively in terms of an established model based on our relaxation measurements and line width analysis.

4. ^{129}Xe line widths

Data on line widths at three magnetic field values and a temperature of 1.4 K are presented as a function of initial mixture O_2 mole fraction in Fig. 2. As mentioned previously, the small intrinsic widths of only 0.03 mT for the pure solid results from the large lattice constant associated with the weak binding of the rare gas solids and the weak magnetic moment of the ^{129}Xe, about 1/4 that of the proton. This intrinsic width consists of both homogeneous and inhomogeneous broadening components from the ^{129}Xe and ^{131}Xe isotopes, respectively. At high concentrations of O_2, additional inhomogeneous line width is encountered. In general, the resultant line width from combined homogenous and inhomogeneous contributions is given by the square root of the sums of the component squares. In our case, there are three components, not all separable, but we employ this protocol, even though it may not be totally justifiable, over the full range of O_2-induced broadening. Our focus is on the higher values of O_2 concentration, where the O_2 contribution to the line width strongly dominates, and where flaws from compounding various line-broadening contributions become negligible. In the low O_2 concentration region, where significant differences might occur, the O_2 contribution to the line width gives no meaningful measurement, since the dispersion of the experimental width determinations considerably exceeds the O_2 contribution to the line width. It should be noted that the line width in the limit of zero O_2 concentration is about 0.032 mT for the lower field values, and about 0.045 mT for the highest magnetic field value (0.96 T). This increase results from the electromagnet's inhomogeneity over the 2 cm length dimension of the condensed sample.

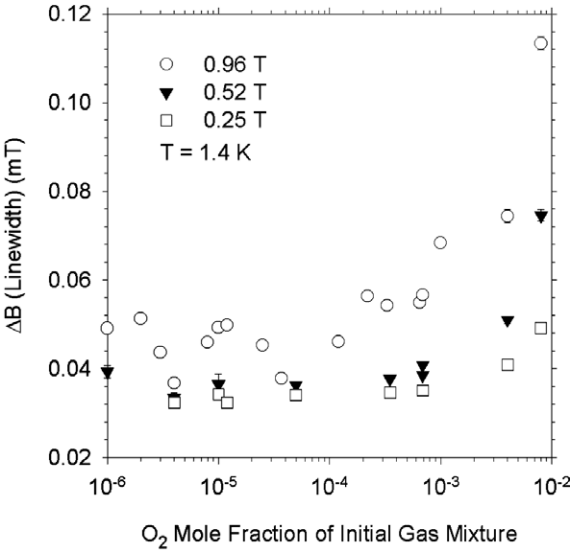

Fig. 2. Measured line width vs. initial mixture O_2 mole fraction at 1.4 K and at three magnetic fields. Widths are between inflection points of derivative scan recordings.

When we consider the dependence of the O_2-induced excess line width on T and B, we are led to a particular model which explains the results in a natural way. Here, the experimental data come from a single sample, and variations arising from differences in the crystal growth conditions of the solid condensed samples, such as seen in Fig. 2, are absent. The magnetic effect of the paramagnetic O_2 on the linewidth of the ^{129}Xe NMR depends on the lifetime of a magnetic state of an O_2 molecule. If the lifetime is long compared with T_{2n} of the ^{129}Xe nuclei, the O_2 magnetic moments act as *static* field sources, with the number within the distribution in any particular magnetic state proportional to the Boltzmann factor for that particular state. The sum of the fields (z component) of all these moments gives a calculable spread of local fields which gives the line shape (and width). A feature of this static distribution is that a considerable residual line width exists even when the B/T ratio is so low that there is no significant net magnetization from the O_2 molecules. On the other hand, if the lifetime of the magnetic state of the O_2 is short compared to T_{2n}, then for the purposes of line broadening, the same average moment associated with the Boltzmann probabilities of the magnetic substrates is found at each O_2 site, and

the effect on the ^{129}Xe broadening is quite different, in fact giving no broadening in the limit of the O_2 magnetization going to zero. Our results strongly suggest that the latter is the prevalent condition, with the short magnetic state lifetimes due to a short $T_{1e}^{O_2}$, and consequently equally short $T_{2e}^{O_2}$, even at low O_2 concentrations. This choice is favored because of implications from the linewidths and from the relaxation model behavior over a large O_2 concentration range.

If the ^{129}Xe excess line width is proportional to the local field produced from summing the fields produced by identical O_2 magnets (Boltzmann time averaged state contributions) at random sites, it will be proportional to the magnitude of the effective O_2 magnetic moment. If the O_2 molecule is in a ground $S = 1$ state, in the absence of other than Zeeman terms in the Hamiltonian, it would have an average effective magnetic moment proportional to the Brillouin function[16] for an $S = 1$ spin, or

$$\mu_{z,\mathrm{eff}} = m = gS\mu_B B_S(x), \tag{1}$$

with the Brillouin function $B_S(x)$ given by

$$B_S(x) = \left(\frac{2S+1}{2S}\right)\coth\left(\frac{2S+1}{2S}x\right) - \left(\frac{1}{2S}\right)\coth\left(\frac{x}{2S}\right) \tag{2}$$

and

$$x = \frac{gS\mu_B B}{k_B T}. \tag{3}$$

In Fig. 3, the excess width for a high O_2 concentration sample as a function of B/T is plotted at two different temperatures. A fit of the points to a spin 1 Brillouin function is poor, and well outside experimental error limits. However, when the crystal field perturbation term $D[Sz^2 - (1/3)S^2]$ is added to the Zeeman terms in the Hamiltonian, and the values of the O_2 magnetic moments are taken into account, using $g = 2.0$, $S = 1$ and optimizing with D as an adjustable parameter, an excellent fit at both temperatures is obtained, yielding $D = 0.19$ meV, or k (2.3 K), where k is Boltsmann's constant. In what follows, we will omit the k and refer to these energies in terms of their Kelvin temperature values.

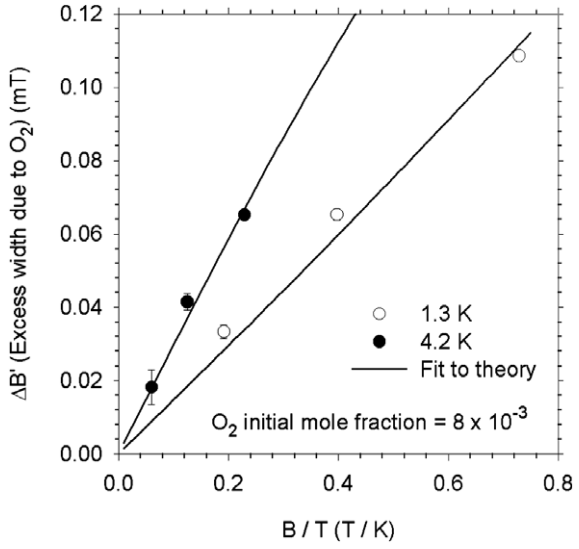

Fig. 3. Plot of O_2-induced excess ΔB against B/T for relatively high initial mixture O_2 mole fractions, at $T = 1.3$ K and 4.2 K. Solid lines are fits determined from $\mu_{z,\mathrm{eff}}$, with optimized value of the crystal field parameters D (2.3 K) and E (0 K). See text.

The magnetic levels of the O_2 molecules including the crystal field terms are illustrated in Fig. 4a, using the value $D = 2.3$ K, determined from the line width analysis, and $E = 0$. The average effective magnetic moment, $\mu_{z,\mathrm{eff}}$, is determined from the Boltzmann distribution populations of the non-equally spaced levels weighted by the z component of the magnetic moment associated with each level:

$$\mu_{z,\mathrm{eff}} = 2\mu_B \frac{\exp\left(\frac{2\mu_B B - D}{kT}\right) - \exp\left(-\frac{2\mu_B B + D}{kT}\right)}{1 + \exp\left(\frac{2\mu_B B - D}{kT}\right) + \exp\left(-\frac{2\mu_B B + D}{kT}\right)}. \tag{4}$$

We can compare the experimental value of the excess line width with the line width calculated from a simulation of an assembly of magnetic moments of identical $\mu_{z,\mathrm{eff}}$. The experimental point chosen for this is the measurement at 1.4 K and 0.96 T with initial mixture oxygen mole fraction 0.0080, where the experimental excess line width value is least subject to complications from compounding of line width contributions, and where the experimental error is only about 5%. We note the width value (measured between inflection points from the derivative recorded spectrum) from Fig. 2 is 0.113 mT, which corrected to excess line width yields a value of 0.105 mT. The line shape is closely Lorentzian, which converts to a FWHM line width (full width at half max) of 0.18 mT. For the simulation, we used 10^5 random sites spaced on an fcc lattice of lattice constant 0.6132 nm, constrained to correspond to the true concentration of the O_2 molecules, in this case 0.32×0.0080, or 0.0026, where it is reminded that the factor 0.32 is the fraction of the initial mixture mole fraction actually incorporated into the condensed solid, as discussed earlier. The simulation also produces a near-Lorentzian shape, with a FWHM line width of 0.26 mT. This is an average of 4 independent simulations, with about a 5% dispersion among them. The discrepancy of about 35% between the simulations and the experimental value is somewhat larger than the estimated errors, but the agreement is close enough to give confidence in the model and in determinations of O_2 concentrations from measured line widths in appropriate ranges of concentration.

There is precedent for the presence of the D term in the magnetic Hamiltonian of O_2 doped rare gas solids from low temperature experiments on heat capacity. Even in the absence of a magnetic field, the D term results in a Schottky anomaly [17] in the heat capacity. Experiments were done on argon, krypton, and several other hosts, but not xenon, so we cannot directly compare our values. However, in Kr, the D value [18] is about 2 K, fairly close to ours in xenon. There is also implication of some residual

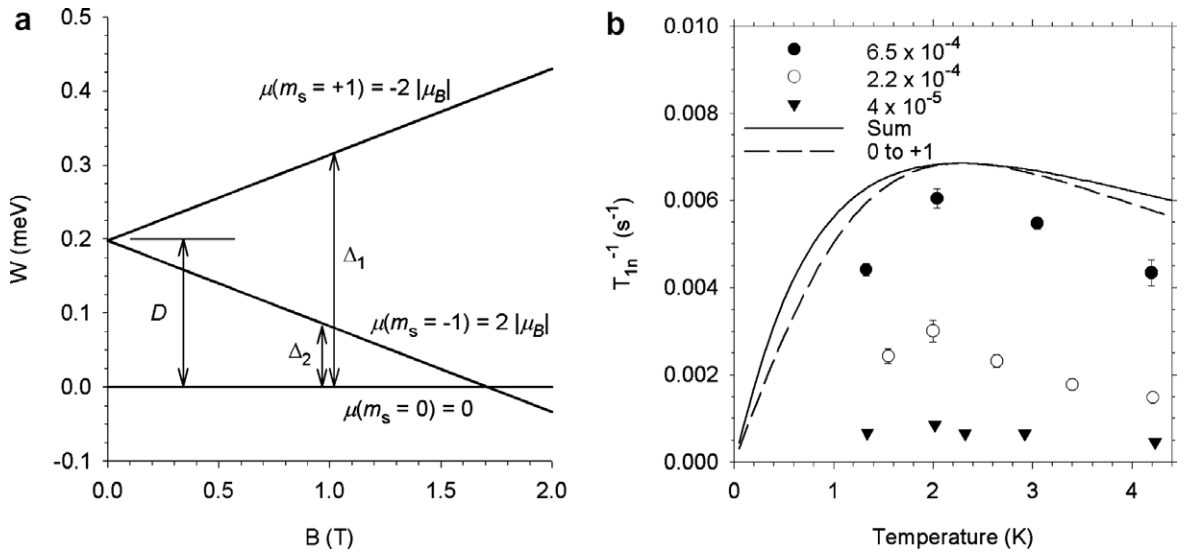

Fig. 4. (a) Energy levels of O_2 in solid Xe vs. magnetic field B. A negligible value of the crystal field parameter E is assumed. (b) Comparison of theoretical model for T_{1n}^{-1} with experimental relaxation data at B = 0.96 T in the 1.4–4.2 K temperature region. Dashed line corresponds to the calculated relaxation rate due to the $0 \rightarrow +1$ O_2 electronic transition for an initial mixture oxygen mole fraction of 6.5×10^{-4}. Solid line is the sum of calculated relaxation rates contributed by all four relevant transitions. τ_e at Δ_1 has been adjusted in each case to maximize T_{1n}^{-1} at 2.3 K. Experimentally measured values of T_{1n}^{-1} at 0.96 T for an initial mole fraction of 6.5×10^{-4} are shown, along with those of two other impurity concentrations.

rotational oxygen molecular motion [23] in these samples, which could be responsible for the short T_{1e} values in all of our samples if the crystal field perturbations alone are insufficient. If so, it would not be likely to contribute significantly to the effective molecular magnetic moment.

5. Low temperature ^{129}Xe spin–lattice relaxation due to O_2

The theory of spin–lattice relaxation in solids with paramagnetic impurities was given in its basic form by Bloembergen [15]. When the concentration of the paramagnetic impurities is low enough so that most of the nuclear spins are too distant to feel the direct magnetic perturbation from the closest paramagnetic impurity, their magnetization can nevertheless change (relax) through spin diffusion via nuclear spin flip-flops with nuclei close enough to the paramagnetic impurity for their T_{1n} to be substantially shortened. Because the flip-flops must conserve energy within the nuclear dipole–dipole reservoir for effective diffusion, spin-diffusion from nuclei too close to the paramagnetic impurity have too large a perturbation of their magnetic energy for effective spin diffusion to the more isolated nuclei. This defines a "barrier" length, δ, one of 3 length parameters relevant to the theory of the relaxation. The other two are the average distance between paramagnetic impurities, R, and the pseudopotential distance [19,20], b, which enters as a necessary 'length' parameter for the solution of the diffusion differential equation. Several modifications of the theory [19–21] were presented in the decade following Bloembergen's original paper. We will follow the treatment of Khutsishvili [20], where the various lengths are well defined, and a quantitative value of the diffusion constant, D, is given for summation over a fcc lattice. Even though his calculation is for a regular lattice rather than the necessarily random distribution over fcc crystal sites as occurs in our case because of the isotopic mixture of natural xenon (26% ^{129}Xe), we nevertheless use the formulas developed by Khutsishvili, with some justification provided by the low sensitivity of calculated T_{1n} to modest variations in D for the rapid-diffusion mode.

Theoretical expressions [20] are given below for nuclear spin relaxation in two principal modes, denoted by *rapid-diffusion*, and *diffusion-limited*. In the former, diffusion spreads the magnetization throughout the sample, but the factor limiting the overall nuclear relaxation rate is the direct relaxation rate of those molecules situated just beyond the diffusion barrier, δ. In the diffusion-limited mode, the direct magnetization rate of nuclei beyond the barrier and thus in spin diffusive contact with the large body of isolated nuclei is rapid compared to the magnetization spread by diffusion, so the diffusion bottleneck sets the overall relaxation rate. The applicable mode depends on the length parameters and on the lifetime of the spin state, τ_e, of the paramagnetic impurity. The rapid diffusion case is associated with $b \ll \delta$, and the diffusion-limited case with $b \gg \delta$. From estimation of the parameters of our system, we expect the rapid-diffusion case to apply here. This will be confirmed when the relevant parameters are derived from our data.

The elements in the theoretical derivation [15,19–21] of the nuclear spin relaxation are briefly summarized. These are the direct nuclear spin-relaxation due to the paramagnetic impurities, the spin diffusion process for nuclei out of range of the direct process represented through the diffusion constant D, the diffusion barrier distance, δ, the pseudopotential[19,20] distance, b, and the average distance between paramagnetic impurities, R, determined

from $(4\pi/3)R^3 = N^{-1}$, where N is the paramagnetic impurity concentration. The direct relaxation rate is given by

$$\frac{1}{T_{1n}}(\text{direct}) = \frac{C}{r^6}, \tag{5}$$

where neglecting angular dependencies,

$$C = \frac{2}{5}(\hbar\gamma_I\gamma_S)^2 S(S+1)\frac{\tau_e}{1+\omega_I^2\tau_e^2}. \tag{6}$$

I and S are the nuclear and electronic spin quantum numbers, γ_I the nuclear magnetogyric factor, ω_I the nuclear Larmor angular frequency in magnetic field B, equal to $\gamma_I B$, and τ_e the lifetime of the electronic spin state, determined from its spin–lattice relaxation time, T_{1e}, and its spin–spin relaxation time, T_{2e}. In our case, as a consequence of the linear dependence of T_{1n}^{-1} (see Fig. 1b) on the O_2-concentration down to the 10^{-5} range implying concentration independence of τ_e, we can exclude T_{2e}^{-1} dominance and conclude the electronic spin–lattice relaxation rate dominates for all the measurements throughout the O_2 concentration range. Thus, T_{1e} can freely substitute for τ_e.

Although it is deduced from our line width analysis and from the low temperature relaxation measurements over the wide concentration range (see Figs. 1a and c) that $\tau_e < T_{2n}$, unlike the case where the static field produced by the time-average values of $\mu_{z,\text{eff}}$ determined the linewidths, for the relaxation it is the power spectrum generated by the fluctuating moments which gives the relaxation mechanism, and the full μ_z associated with the energy levels undergoing transitions is relevant. Thus for the relaxation case, Eq. (6) can be written

$$C = \frac{2}{5}(\hbar\gamma_I)^2\left(\frac{2\mu_B}{\hbar S}\right)^2\frac{\tau_e}{1+\omega_I^2\tau_e^2}. \tag{6a}$$

We rewrite Eq. (6a) with a slight rearrangement

$$C = \frac{2}{5}(\gamma_I)^2\frac{4\mu_B^2}{S(S+1)}\left(\frac{1}{\omega_I}\right)\frac{\omega_I\tau_e}{1+\omega_I^2\tau_e^2}. \tag{6b}$$

In this form, the maximum in the τ_e term at $\omega_I\tau_e = 1$ is seen explicitly.

The spin diffusion constant, D, is approximated [20] for a fcc lattice by

$$D = \frac{1}{14}a^2T_2^{-1}. \tag{7}$$

The unit cell lattice parameter [22] of 0.632 nm gives a nearest neighbor distance $a = 0.447$ nm for xenon. With T_2, the ^{129}Xe spin–spin relaxation time, of approximately 0.5 ms, determined from the nuclear spin resonance linewidth, D is about 28 nm^2 s^{-1}, independent of B and T, except possibly at the highest concentrations.

The pseudopotential distance is given by

$$b = 0.68\left(\frac{C}{D}\right)^{1/4}. \tag{8a}$$

It has weak B and T dependencies through the C factor. At $T = 2.3$ K and $B = 0.96$ T, where, as will be shown below, $\tau_e = 1.4\times10^{-8}$ s,

$$b = 5.4\times10^{-10}\tau_e^{-1/4} = 0.49\text{ nm}. \tag{8b}$$

The diffusion barrier distance, δ, is defined as that distance from the paramagnetic impurity where the perturbing field is of the order of the local nuclear dipolar (dd) field, or where

$$\frac{\mu_{z,\text{eff}}}{\delta^3} = \Delta B_{\text{dd}}. \tag{9a}$$

Under these conditions, the parameter δ^3 would be linearly dependent on magnetic field B, through the $\mu_{z,\text{eff}}$ term in Eq. (9a). However, while the time averaging over the spin states which produces $\mu_{z,\text{eff}}$ appears applicable to the static line widths of the xenon spins, it is not obvious that this averaging applies to the spin–spin flip-flopping associated with the spin diffusion. A time-averaged magnetic moment which sources an effectively static magnetic field producing line widths does not necessarily average the same way when it functions to inhibit, with the inhomogeneous fields it produces, energy conserving flip-flop transitions involved in spin diffusion. In the latter case, δ can have a different dependence on magnetic field. We defer further consideration of the magnetic field dependence of δ^3 until direct comparison of the experimental results with the theory is made. With $\mu_z = 2\mu_B$, a representative value for our system in the light of uncertainties expressed above, and with $\Delta B_{\text{dd}} = 0.03$ mT, we get

$$\delta = 4.0\text{ nm}. \tag{9b}$$

The parameter R, indicative of the average separation [20] of O_2 impurities, is given by

$$R = \left(\frac{3}{4\pi N}\right)^{1/3} \tag{10}$$

where N is the true O_2 concentration. For a particular initial mixture oxygen mole fraction of 6.5×10^{-4}, or true O_2 mole fraction of 2.0×10^{-4}, N is equal to 3.6×10^{24} m^{-3}, and $R = 4.1$ nm.

The nuclear relaxation times for the diffusion limited case and the rapid diffusion case are given by Khutsishvili [20] as

$$T_n = 1.6\frac{(bR)^3}{C}, \quad \text{for } b \gg \delta \text{ (diffusion-limited)}, \tag{11}$$

and

$$T_n = \frac{(\delta R)^3}{C} \text{ for } b \ll \delta \text{ (rapid-diffusion)}. \tag{12}$$

From comparison of Eqs. (8b) and (9b), it is seen that the rapid-diffusion mode is applicable, and that even an order of magnitude decrease in D, for example from having neglected isotopic dilution of ^{129}Xe in the lattice, would not

invalidate the inequality condition for rapid-diffusion. The temperature and magnetic field dependencies for rapid-diffusion relaxation are distinctly different [21] from those of the diffusion-limited case. From Eq. (12), which corresponds to the rapid-diffusion mode, the relaxation rate is proportional to NC (N is proportional to R^{-3}), and temporarily excluding any B dependence of δ as proposed following Eq. (9a) in the text, the T and B dependencies of the nuclear relaxation rate come from the C term, displayed in Eq. (6b). Typical electronic relaxation in the liquid helium temperature region involves coupling of the spin system to the phonon energy reservoir in a first order phonon process, with $T_{1e}^{-1} \propto TB^2$. This is for simple Zeeman energy level separations, which are proportional to B. However, with the crystal field term present as shown in Fig. 4a, the energy separations of levels at a given field are no longer proportional to B. In fact, at a given field, there are four different fluctuating fields due to transitions which produce separate power spectra and whose induced nuclear relaxation rates add. Denoting the separation of energy states at a given field value as Δ_1 and Δ_2, as shown in Fig. 4a, for the $[0 \rightarrow +1,\ +1 \rightarrow 0]$ and the $[0 \rightarrow -1,\ -1 \rightarrow 0]$ transitions respectively, the first order phonon relaxation process is based on those energy separations, and thus $T_{1e,i}^{-1} \propto T\Delta_i^2$. We note that the rates associated with Δ_1 and Δ_2 are quite different in the field-temperature range we use, and that their *variations* with change of B are in opposite directions. We also take note that the rates for $0 \rightarrow +1$ and $+1 \rightarrow 0$ [also $0 \rightarrow -1$ and $-1 \rightarrow 0$] are very different for large Boltzmann factor. The Boltzmann factor slows down the transition rate of the lower level to higher level states, which assures the Boltzmann population difference. This occurs because the low to high level transition requires excited phonon states whose populations also decrease by the Boltzmann factor.

We facilitate the analysis connecting this theoretical framework to the experimental data by taking advantage of three distinct special experimental features of the measurements. These are the anomalous T_{1n}^{-1} vs T behavior, shown in Fig. 1d for a field of 1 T, which exhibits a maximum at about 2.3 K; the occurrence of this same general temperature dependence at fields of 0.25 and 0.5 T, with a T_{1n}^{-1} maximum between 1 K and 2 K; and the approximate field *in*dependence of T_{1n}^{-1} over the 1.4–4.2 K temperature range. The first feature producing a T_{1n}^{-1} maximum at 2.3 K is readily accommodated by setting $\omega_I\ \tau_e = 1$, thereby providing directly the value of τ_e, which is otherwise difficult to obtain with magnetic resonance measurements. With $\omega_I = 7.15 \times 10^7\ s^{-1}$ at 0.96 T, this produces the result used earlier that $T_{1e} = 1.4 \times 10^{-8}$ s. The second feature, T_{1n}^{-1} showing a similar maximum at T between 1 K and 2 K at other fields, is accounted for if τ_e^{-1} is approximately proportional to ω_I, or B. The transition which does behave this way, with in fact Δ_1 approximately proportional to $B^{1/2}$, is $0 \rightarrow +1$, so we hypothesize its dominance. Its effective relaxation rate, $W_{0\rightarrow1}$, obtained from Eqs. (6b), [12] and [10], is given by

$$W_{0\rightarrow1} = \frac{2}{5}(\gamma_I)^2 \frac{4\mu_B^2}{S(S+1)} \left(\frac{1}{\omega_I}\right) \frac{\omega_I \tau_e}{1+\omega_I^2\tau_e^2} \times \frac{4\pi N}{3\delta^3}. \quad (13)$$

It is plotted as the dashed line in Fig. 4b, with $S = 1$, and corresponds to initial mixture oxygen mole fraction of 6.5×10^{-4} ($N = 3.6 \times 10^{24}\ m^{-3}$). The agreement in magnitude with the experimental value at the corresponding value of N is close, probably fortuitously so considering the uncertainties in some of the theoretical quantities. T_{1n}^{-1} values corresponding to samples of different O_2 concentrations are also plotted. The variations from a strict N dependence arise from the dispersion of up to a factor of 2 in T_{1n}^{-1} proportionality to N, as seen in Fig. 1b. The non-monotonic T dependence of T_{1n} on temperature of the theoretical curve follows reasonably well the T dependence of the experimental data for all concentrations. We can also include the other Δ_i transitions, whose W values are linked to $W_{0\rightarrow1}$ through the dependence on their relative Δ values, taking into account also the previously noted decrease in transition rate of $W_{0\rightarrow1}$ with respect to $W_{1\rightarrow0}$ by the Boltzmann factor $\exp(-\Delta_1/kT)$. This holds similarly for the $(0 \rightarrow -1,\ -1 \rightarrow 0)$ transitions. Multiplying the W values by their respective initial state populations and adding them gives W_{SUM}, which is also plotted in Fig. 4b as a solid line. One adjustable factor, τ_e at Δ_1, positions the maximum near 2.3 K. Thus, the theoretical calculations produce a reasonable fit to the data, which support the premises and concepts of the theoretical model. The third special experimental feature, approximate field *in*dependence of the T_{1n}^{-1} values in the temperature-field region investigated, is still not accounted for. By keeping $\omega_I\tau_e$ approximately constant with changing field, the 2.3 K maximum nuclear relaxation rate increases as $1/\omega_I$, or $1/B$, as seen in Eq. (13). This can be compensated by assigning an inverse field dependence to δ^3. Such an inverse dependence on B may arise from the approximate proportionality of ΔB_{dd} to B, in conjunction with Eq. (9a). This is suggestive, but other factors may also be involved in the complex spin diffusion process in an inhomogeneous magnetic field. In summary, an interesting model with some novel features accounts for the relaxation dependencies of T_{1n}^{-1} on field, temperature and paramagnetic impurity concentration in the low temperature region. In Section 6.2 below, a plausible case is presented for extrapolations into the higher temperature and higher field regions, which can impact on production of hyperpolarized ^{129}Xe for room temperature usage.

6. Discussion

Two aspects of this work warrant additional discussion. The first concerns the methods of preparation of the matrix isolated impurities and the effort to correlate the initial gaseous component mixtures with their actual concentrations in the condensed state through the excess width and T_{1n}^{-1} measurements. The second concerns what inferences can be drawn from the present results regarding the production and use of hyperpolarized ^{129}Xe.

6.1. Concentration of O_2 in solid xenon

We have used two methods to incorporate various concentrations of O_2 in solid xenon. The first is a fairly rapid freeze of a gaseous mixture of Xe and O_2, similar to the most common methods for producing matrix isolated impurities. In the second method, which is more tractable in a situation where the solute is more volatile than the solvent, such as the xenon + O_2 mixtures which are under consideration here, a liquid phase is first condensed, followed by a moderately rapid freeze over a typical period of about 3–10 min. The dynamics of the two methods are quite different. As mentioned previously, the latter generally results in better crystals and smaller line widths. Both methods yield mixtures in the solid proportional to the initial gas mixture, but few past studies have actually established the actual concentrations. Our choice of xenon makes this possible through the excess line width dependence on actual impurity concentration, and to a lesser extent, from the possibility to infer an absolute impurity concentration from the T_{1n}^{-1} values at low temperatures.

With our model of the magnetic ground levels of the O_2 impurities, and with the assumption of $T_{1e}^{O_2} \ll T_{2n}^{Xe}$, we assign a known and identical average moment to each of the impurities located on random sites of a fcc lattice, and sum them over a sufficient volume to get a distribution which leads to a line broadening for a given concentration. This is compared with the experimentally observed excess line width. Such simulations implied a concentration in the samples which were first liquefied about a factor of 3 less than what would correspond to the initial gas mixtures. In fact, the mechanism of O_2 going into solution is fairly complicated. During the condensation, volatile oxygen forms a barrier[11] which prevents complete condensation of the xenon, which depends on the volumes and shape of the apparatus in which condensation occurs, and on the mole fractions in the gas mixture. The oxygen partial pressure in the barrier region above the condensation volume can be the determinant, through Henry's law, of the amount of the O_2 which goes into solution, and the time for a hopefully homogeneous diffusion throughout the liquid phase as well as the temperature-dependent maximum solubility of the O_2 in the xenon are important factors. We have engaged in limited experimentation with this process, but in this paper, we simply note that we generally waited a time of about 10 min for adequate diffusion into the liquid during which time the barrier pressure did not undergo much change. It would seem likely that for most of the experiments, less O_2 entered the solid than would correspond to the initial gas mixture. For the direct freezing, bypassing the liquid state, the excess line width measurements suggest a greater disparity from the initial mixture amount.

We eventually measured the true O_2 mole fraction in the Xe–O_2 solid in a fairly simple manner, making use of the barrier effect [12]. An auxiliary side tube into which the gas mixture could be condensed was calibrated to allow O_2 mole fraction determination via the barrier effect. This also served to monitor any changes in oxygen mole fraction for gas mixture samples retained over long periods. The condensed solid in this auxiliary barrier effect tube is warmed up, and the gas mixture is subsequently condensed as a liquid in the experimental apparatus. During the subsequent freezing of the liquid sample, the temperature is lowered to about 100 K, where the vapor pressure of the solid is less than 100 Pa. The excess gas (due to a barrier effect in the *experimental apparatus*) is pumped away. Upon re-heating, and then re-condensing in the auxiliary barrier-effect side tube, the measured O_2 mole fraction reflects the actual O_2 concentration of the solid sample which had been condensed in the experimental apparatus. This procedure was carried out for two initial mixture O_2 mole fractions, 2×10^{-3} and 7×10^{-4}, and in each case, the mole fraction in the sample condensed in the experimental apparatus by our described protocol was reduced by a factor of 3.2, as discussed previously in the paper, with an estimated error of 10%. Taking account of this factor led to fair agreement (about 35%) between the measured ^{129}Xe excess line widths and the values generated by the simulations.

Eq. (12) yields a relation between T_{1n} values at low temperature and actual O_2 concentration values, N. The relation however involves an unknown parameter τ_e, the electronic spin relaxation rate, and so Eq. (12) cannot be used alone to calibrate O_2 concentrations. However, the remarkable experimental fact of the maximum at 2.3 K of T_{1n}^{-1} with respect to T in the 1.4–4.2 K region does give a value of τ_e in terms of the nuclear Larmor frequency, ω_I. Oxygen concentrations can now be calculated and compared with the values obtained from the line widths, and from the independent gas constituent determinations described above. If τ_e could be measured directly by an independent method, such as ESR, it could provide another way to corroborate true O_2 concentrations in the solid.

6.2. Routes to hyperpolarization

Hyperpolarized ^{129}Xe has many applications, and can be prepared in various ways. We confine the discussion here to obtaining the hyperpolarized xenon in the gaseous state at room temperature, with a relaxation time [24] (depolarization time) of the order of minutes, in a modest holding field of the order of a hundred gauss.

A simple production of modest hyperpolarization, not requiring any oxygen removal, was demonstrated. Using an initial mixture O_2 mole fraction of about 0.01% (which overlaps the oxygen concentration (corrected) region where polarization of about 0.1 was obtained in a few days in the mK — multi-tesla environment [1]), hyperpolarized xenon with an enhancement close to 10^2 was obtained operating between 1.4 K and 150 K. Referring to Fig. 1a, at 0.01% initial mixture O_2 mole fraction, the T_{1n} values at 1.4 K and 150 K are respectively about 20 min and 10 min. In the absence of O_2, the T_1 of ^{129}Xe at 1.4 K would be several

hours and to build up to 95% polarization would require a time of $\sim 3T_1$, or about 10 h, whereas with the modest O_2 concentration, 95% polarization is achieved in about an hour. At the higher temperature, even without removal of the O_2, T_{1n} is long enough for hyperpolarized MRI measurements, and it is feasible to vaporize rapidly the solid for an application involving the spin polarized gas. Even at 0.01% true O_2 mole fraction and 300 K, the T_1 of ^{129}Xe in the gas phase[24] is about 3 min, sufficient for many applications. By employing field cycling to 8 T in an ordinary liquid helium cryostat, one should be able to boost the enhancement to 10^3. With the dilution refrigerator, expected enhancements rise to 10^4. At higher oxygen concentrations and variant extraction protocols, there may be room for further improvement in the ultimate hyperpolarization attainable. The Nottingham group[9] tried oxygen concentrations which they concluded were too high for retrieval to high temperatures without excessive depolarization. Between our concentration and theirs, there is room for appreciable hyperpolarization. Dynamic nuclear polarization (DNP) of the ^{129}Xe at temperatures between 0.4 K and 1.4 K, followed by the warm-up phase, is an alternate route. Some DNP enhancement has recently been achieved by our group at 1.5 K and 0.3 T, and work on this is actively being pursued. Nitrogen dioxide is in the class of oxygen, to the extent it is a gaseous radical which is removable. Other examples include light-induced paramagnetic impurities acting through HI or HBr, which in some cases provide a relaxation switch simply by turning on and extinguishing a light source.

High concentrations of paramagnetic impurities for more efficient low T polarization must be removed before they too quickly depolarize the xenon at higher temperatures. Several possibilities are suggested from our investigation. Though T_{1n} values at high field have not yet been measured in the temperature region between 1 K and room temperature, the known aspects of the relaxation suggest that the paramagnetic impurities will not further increase depolarization at higher temperatures and at higher magnetic fields. The electronically induced fluctuation power spectrum is already making maximum contribution to T_{1n}^{-1} at 2.3 K, so increasing T, at least up to 100 K, should not increase T_{1n}^{-1}, as is supported by data shown in Fig. 1a. In fact, higher fields should probably reduce the paramagnetic impurity contribution to the nuclear relaxation, for expected changes of T_{1e} with increasing field. This is favorable, since the relaxation rate caused by the vacancy mechanism at higher temperatures is also reduced at higher fields, and advantage can be taken of that provided the O_2 impurities do not make matters worse. Thus, warming up in high fields could be expected to result in reduced depolarization. Other approaches may include raising the temperature of hyperpolarized Xe at high pressures to supercritical temperatures, which could reduce the warm-up time by delaying the liquid xenon melting. A report of a manageable intrinsic polarization in this state exists [25], and it is reasonable for this high temperature liquid under pressure to retain a satisfactory T_1. Furthermore, at almost any stage, vaporization of the O_2–Xe solid mixture with subsequent cryo-trapping of the xenon while the system is pumped provides an oxygen removal route. We have made preliminary experiments of this nature with some encouraging results.

References

[1] A. Honig, X. Wei, A. Lewis, E. ter Haar, K. SerajiGozogzad, LT22, Physica B 284–288 (2000) 2049.
[2] W. Happer, E. Miron, S. Schaefer, D. Schreiber, W.A. von Wijngaarden, X. Zeng, Phys. Rev. A 29 (1984) 3092.
[3] M.S. Albert, G.D. Cates, B. Dreihuys, W. Happer, B. Saam, C.S. Springer Jr., A. Wishnia, Nature (London) 370 (1994) 199.
[4] M.R. Adams et al., Phys. Rev. D 50 (1994) 1836.
[5] A.S. Verhulst, O. Liivak, M.H. Sherwood, H-.M. Vieth, I.L. Chuang, Appl. Phys. Lett. 79 (2001) 2480.
[6] A. Honig, Bulk production and usage of hyperpolarized ^{129}Xenon, US Patent #6125654.
[7] See, for example Raymond S. Alger, Electron Paramagnetic Resonance, Interscience Publishers, John Wiley and Sons, 1968.
[8] W.M. Yen, R.E. Norberg, Phys. Rev. 131 (1963) 369.
[9] E.V. Krjukov, J.D. O'Neill, J.R. Owers-Bradley, J. Low Temp. Phys. 140 (2005) 397.
[10] For a concise discussion of these terms, see S.P. McGlynn, T. Azumi, M. Kinoshita, Molecular Spectroscopy of the Triplet State, Prentice Hall, New Jersey, 1969.
[11] J.C. Burford, G.M. Graham, Can. J. Phys. 47 (1969) 23.
[12] C. Kenty, Rev. Sci. Instrum. 17 (1946) 158.
[13] N.N. Kuzma et al., Phys. Rev. Lett. 88 (2002) 147602.
[14] K.P. Wong, J. Magn. Res. 1 (1969) 55.
[15] N. Bloembergen, Physica XV 386 (1949).
[16] See, for example C. Kittel, Introduction to Solid State Physics, 4th ed., John Wiley and Sons, NY, 1971.
[17] J.C. Burford, G.M. Graham, J. Chem. Phys. 49 (1968) 763.
[18] J.C. Burford, G.M. Graham, J. Chem. Phys. 52 (1970) 5225.
[19] P.G. DeGennes, J. Phys. Chem. Solids 7 (1958) 345.
[20] G.R. Khutsishvili, in: C.J. Gorter (Ed.), Progress in Low Temperature Physics, vol. 6, North Holland, Amsterdam, 1970, p. 375.
[21] W.E. Blumberg, Phys. Rev. 119 (1960) 79.
[22] P.R. Granfors, A.T. Macrander, R.O. Simmons, Phys. Rev. B 24 (1981) 4753.
[23] P.I. Muromtsev, M.I. Bagatskii, V.G. Manzheli, I.Ya. Minchina, Low Temp. Phys. 20 (1994) 195.
[24] C.J. Jameson, J. Chem. Phys. 89 (1988) 4074.
[25] M. Haake, Chem. Phys. Lett. 292 (1998) 686.